Bruggemann, Troy S., Ford, Jason J., & Walker, Rodney A. (2010) ***Control of aircraft for inspection of linear infrastructure. IEEE Transactions on Control Systems Technology***.

Control of Aircraft for Inspection of Linear Infrastructure

Troy S. Bruggemann, Jason J. Ford and Rodney A. Walker, *Member, IEEE*

***Abstract*—Inspection aircraft equipped with cameras and other sensors are routinely used for asset location, inspection, monitoring and hazard identification of oil-gas pipelines, roads, bridges and power transmission grids. This paper is concerned with automated flight of fixed-wing inspection aircraft to track approximately linear infrastructure. We propose a guidance law approach that seeks to maintain aircraft trajectories with desirable position and orientation properties relative to the infrastructure under inspection. Furthermore, this paper also proposes the use of an adaptive maneuver selection approach, in which maneuver primitives are adaptively selected to improve the aircraft's attitude behaviour. We employ an integrated design methodology particularly suited for an automated inspection aircraft. Simulation studies using full nonlinear semi-coupled six degree-of-freedom equations of motion are used to illustrate the effectiveness of the proposed guidance and adaptive maneuver selection approaches in realistic flight conditions. Experimental flight test results are given to demonstrate the performance of the design.**

***Index Terms*—Aircraft control, adaptive maneuver selection, guidance, linear infrastructure, power line inspection.**

I. Introduction

AIRCRAFT equipped with cameras and other sensors can be used in a significant number of civilian applications such as remote mapping [1], geolocation and feature tracking [2] and remote sensing [3]. Of particular importance amongst these remote sensing applications, are the asset inspection tasks which are costly, time-consuming and tedious (especially when assets are extensive, sparse, or difficult to locate or access). One commonly appearing class of inspection tasks is those involving approximately piecewise linear assets such as oil-gas pipelines, roads, bridges, power-lines, power generate grids, rivers, coastlines, canals, highways and forest fire boundaries [4], [5], [6], [7], [8], [9], [10], [11], [12]. Flying manned or unmanned aircraft fitted with appropriate camera and sensor payloads taking imagery of such infrastructure assets, could save countless man-hours and costs normally associated with asset management, thereby improving the efficiency of the operations. Although low-altitude linear infrastructure inspection applications such as power line surveillance have been studied since the mid-1990's, the need for further remote sensing automation continues to be highlighted by many authors [3], [9], [10], [11], [12], [13], [14], [15].

The purpose of this paper is to investigate flight automation issues for low-altitude fixed-wing inspection platforms tracking linear infrastructure. One key issue for linear infrastructure inspection involves determining a suitable aircraft control approach that ensures aircraft flight with a fixed relative position and relative body attitude with respect to the linear infrastructure under inspection. In typical operation, there is a requirement for downward-looking body-fixed cameras to capture the objects on the ground within their fixed and limited field of view [3], [4], [5], [7], [8], [16], [17].

The principle of operation is that after appropriate flight path selection, the field of view seen by the camera will be flown down the length of the infrastructure under inspection. Unfortunately, any aircraft roll, pitch or yaw will translate the asset's imaged position, and perhaps even move the asset out of the camera's field-of-view. For this reason, minimising roll-motion is an important issue faced by inspection aircraft with body-fixed cameras. Even for inspection aircraft equipped with gimballed cameras, aircraft attitude motion is undesirable [17].

The planning and control of fully autonomous platforms is typically separated into three sub-problems: the trajectory planning sub-problem [19], the guidance sub-problem of tracking the planned trajectory [7], [20], and the autopilot or maneuver sub-problem of following the issued guidance commands [20], [21]. Generic versions of the first of these sub-problems, the trajectory planning problem, have been studied by several researchers and many of the techniques developed can be readily applied to infrastructure inspection. These include explicit planning techniques [19], [17], [22], motion primitive planning techniques [18], and implicit techniques such as those involving virtual waypoints [23].

Early investigations of the second sub-problem, the guidance problem, illustrated that simple PID based control loops (directly based on GPS derived tracking errors) leads to poor cross-track position and velocity performance [4], [24]. In [24], new heading error rate type lateral track controllers were proposed for the Aerosonde UAV and these approaches were illustrated to reject certainty types of wind disturbances. In [4], hardware-in-the-loop experiments illustrated the use of combining image-based information and heading error rate controllers in the problem of tracking road infrastructure. Others [7], [16] have proposed a biased proportional navigation (BPN) guidance approach that used image-based measurements for road tracking. Alternatively, vector field based [25] and Lyapunov approaches [26], have been proposed

T.S. Bruggemann is with the Cooperative Research Centre for Spatial Information and the Australian Research Centre for Aerospace Automation, at the Queensland University of Technology, Brisbane, QLD, 4001 Australia (e-mail: t.bruggemann@qut.edu.au).

J.J. Ford is with the Cooperative Research Centre for Spatial Information and the Australian Research Centre for Aerospace Automation, at the Queensland University of Technology, Brisbane, QLD, 4001 Australia (e-mail: j2.ford@qut.edu.au).

R.A. Walker is with the Cooperative Research Centre for Spatial Information and the Australian Research Centre for Aerospace Automation, at the Queensland University of Technology, Brisbane, QLD, 4001 Australia (e-mail: ra.walker@qut.edu.au).

in a number of slightly modified tracking problems. However, few of these previous guidance approaches rigorously consider both the relative position and orientation of the platform. Furthermore, most fail to consider the impact of maneuver choice on trajectory tracking performance, nor the impact that any tracking error has on the underlying inspection activity.

The third sub-problem, the maneuver problem, has particular importance in the inspection application because aircraft maneuver behaviour can have a significant impact on the inspection task because heading corrections are typically indirectly actuated through aerodynamically efficient bank-to-turn (BTT) maneuvers. That is, in a standard fixed-wing aircraft autopilot configuration, heading adjustments are achieved through banking the aircraft's airframe [27]. Clearly, banking maneuvers are a problematic strategy for inspection platforms because the banking action risks changing the camera's field-of-view too much, causing the asset to no longer be under inspection [8]. One possible avenue for reducing the apparent conflict between heading requirements and banking behaviour emerges from the missile control community where systems are often designed to exploit different maneuver behaviours during different mission phases. Specifically, a missile might gain-schedule between aerodynamically efficient BTT maneuvers during early stages and skid-to-turn (STT) maneuvers for small corrections during terminal stages [28], [29]. This adaptive maneuver selection approach allows the different characteristics of various maneuver regimes to be exploited during different flight stages.

Each of these three sub-problems could be considered in sequential manner. However, separate sub-system design does not often lead to acceptable performance because it cannot exploit any beneficial relationships between the sub-systems [20].

This paper makes three contributions to the autonomous aircraft inspection problem. The first contribution is to propose the use of a precision guidance law that commands towards flight trajectories with desirable position and heading relative to the infrastructure under inspection [30], [31]. This guidance law was originally designed for the purpose of controlling a missile to impact a target at a desired impact angle. In contrast, we investigate the performance of this guidance law for inspection of linear assets where the aim is to intercept and track a desired line of inspection.

The second contribution is to propose an adaptive maneuver approach, inspired by hybrid autopilot designs used in missile autopilots, which aims to achieve guidance commands whilst maintaining desirable attitude behaviour [28], [29]. The inclusion of adaptive maneuver behavior within the aircraft control system allows a greater range of performance characteristics to be exploited. We highlight that care must be taken to ensure that flight stability remains a priority, but these low-level platform-specific issues are not explicitly considered in this paper. However, full autopilot dynamics were used in our simulation studies.

The third contribution is our integrated system design for autonomous control of inspection aircraft. Separate sub-system design does not often lead to acceptable performance whereas an integrated design is often done in military systems such as missile systems [20], [21], [28], [29]. We argue that the absence of a human pilot in the control loop and the particular features of the aircraft inspection problem suggests that the three sub-problems of trajectory planning, guidance and maneuvering should be considered in an integrated manner. We examine the proposed infrastructure inspection approach by experimental flight testing and using simulation studies with high-fidelity aerodynamic models (including all necessary low-level autopilot loops) to illustrate the benefits of the proposed guidance and control concepts.

This paper is organised as follows: In Section II aerodynamic models are introduced and the tracking linear infrastructure for inspection problem is posed in terms of the three sub-problems of trajectory planning, guidance, and maneuvering. In Section III a precision guidance law is presented as a potential solution of the guidance sub-problem. In Section IV an adaptive maneuver approach is presented as a potential solution to the maneuvering sub-problem. In Section V simulation studies using high-fidelity aerodynamic models are presented, as well as results from experimental flight testing. Finally, in Section VI, some brief concluding statements are made.

II. Aircraft Dynamics and the Inspection Problem

The goal of our infrastructure inspection problem is to achieve controlled flight over the infrastructure so that every part of the asset can be seen, at some point during flight, by a limited field of view sensor that is mounted to the aircraft. In this section we describe the dynamics involved in the inspection problem and then introduce three sub-problems that help to solve our aircraft control for linear infrastructure inspection problem.

A. Aircraft Dynamics

Under rigid-body, fixed mass and no wind assumptions, the six degree-of-freedom equations of motion for a fixed-wing inspection aircraft can be expressed in the form [34]:

$$\frac{d\bar{v}^b}{dt} = \frac{F^b(u)}{m} + T_n^b(\Theta)g^n - \tilde{\omega}^b\bar{v}^b \quad (1)$$

$$\frac{d\omega^b}{dt} = \mathcal{I}_b^{-1}\left(M^b(u) - \tilde{\omega}^b\mathcal{I}_b\omega^b\right) \quad (2)$$

with the auxiliary equations

$$\frac{dr^n}{dt} = T_n^b(\Theta)\bar{v}^b \quad (3)$$

$$\frac{d\Theta}{dt} = T_p^e(\Theta)\omega^b \quad (4)$$

where $\bar{v}^b = [u^b, v^b, w^b]'$ are body-fixed velocities, $\omega^b = [p, q, r]'$ are body-fixed rates, $r^n = [x^n, y^n, z^n]'$ are the aircraft's spatial location in some navigation frame, and $\Theta = [\psi, \theta, \phi]'$ are the Euler yaw, pitch and roll angles. Here $F^b(u)$ and $M_b(u)$ and the aerodynamic force and moments, m is aircraft mass, g^n is the local gravity vector in the navigation frame, $\mathcal{I}_b$ is the aircraft's body-axis inertia matrix, $\tilde{\omega}^b$ is the skew-symmetric matrix equivalent for ω^b, and $u = [u_a, u_e, u_r]'$ is the control input where u_a, u_e, and

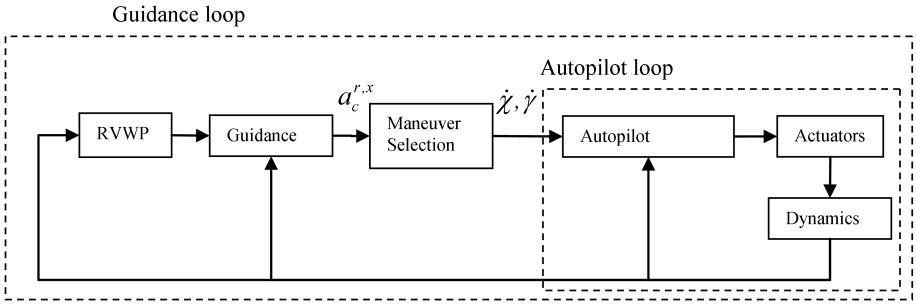

Fig. 1. The RVWP (receding virtual waypoint), guidance, maneuver and autopilot functions.

u_r are aileron, elevator and rudder controls, respectively. We highlight that some secondary $\bar{v}^b$ and ω^b cross-coupling in the $F^b(u)$ and $M^b(u)$ terms has been omitted. More details about aircraft aerodynamics can be found in many references, such as [33].

Quantities expressed in terms of the body-fixed frame will be denoted with the superscript b, as distinct from quantities in the reference or navigation frame which will be denoted with superscript n. The rotation matrix T_b^n is from the body frame to the navigation frame, whilst T_p^e is the transformation matrix from body rates to Euler rates. Finally, we let $r_{a,b}^n$ denote the aircraft position trajectory on the time interval $t \in [a, b)$.

B. Simplified Aircraft Dynamics

Much of the previous research on aircraft trajectory control has made certain assumptions about the Euler angles, so that platform dependent features can be avoided and the inspection problem can be posed on simplified translational dynamics (for example see [19], [36]). However, these approaches have unfortunately ignored many important aircraft attitude issues.

In this paper, we suggest that it is more appropriate to represent inspection aircraft dynamics using a decoupled nesting of the slow translation dynamics around the rotational dynamics. The translation dynamics of the inspection aircraft are described by the rigid body equations (1) and (3), whilst the angular dynamics are described by equations (2) and (4). Decoupling in terms of maneuver primitives seems reasonable because fixed-wing aircraft generally use the same types of maneuvers (even if the individual implementations are different), see [7], [16], [18] for a range of similar ideas. Furthermore, this particular decoupling choice also facilitates practical implementation because commercial autopilot solutions with built-in maneuver modes, such as the MicroPilot^{TM} for micro UAVs, can be used with minimal modification.

Let us assume the inspection aircraft is flying at constant speed. Rather than the full rigid-body equations (1)-(4), we consider the aircraft's translational dynamics to be

$$\begin{aligned} \dot{x}^n &= V\cos\chi\cos\gamma \\ \dot{y}^n &= V\sin\chi\cos\gamma \\ \dot{z}^n &= V\sin\gamma \end{aligned} \tag{5}$$

where V is the magnitude ground speed of the aircraft (assumed constant), χ is the course angle, and γ is the flight path angle.

The dynamics of χ and γ are consider to be a concatenation of maneuver primitives in the sense that, if we let t_i denote the start time of the ith maneuver, then the evolution of χ, γ during the time period $[t_i, t_{i+1})$ is described by the aircraft's maneuver dynamics [19]

$$\begin{aligned} \dot{\chi} &= \frac{1}{mV\cos\gamma}\left[(L+T\sin\alpha)\sin\sigma\right. \\ &\quad \left.+(D-T\cos\alpha)\cos\sigma\sin\beta+Y\cos\sigma\cos\beta\right] \\ \dot{\gamma} &= \frac{1}{mV}\left[(L+T\sin\alpha)\cos\sigma+(T\cos\alpha-D)\sin\sigma\sin\beta\right. \\ &\quad \left.-Y\sin\sigma\cos\beta\right]-\frac{1}{V}g\cos\gamma \end{aligned} \tag{6}$$

where σ is bank angle (rotation about the velocity vector), β is the sideslip angle, α is the angle of attack, L is the lift force, T is the thrust force, D is the drag force, Y is the side force and with the condition for constant velocity $0 = \frac{1}{m}(T\cos\alpha - D) - g\sin\gamma$. Here, the bank angle σ is related to roll angle ϕ through the expression $\cos\sigma\cos\gamma = \cos\alpha\cos\theta\cos\phi + \sin\alpha\sin\theta$ [35].

We will consider maneuver primitives to be feasible stable flight behaviours described by specific choices of α, β, σ, L, T, D, and Y in (6). As an example of stable flight modes that could be used for inspection, a period of straight and level flight can be achieved through choice of u_a, u_e, and u_r controls that achieve $\beta = 0$, $\sigma = 0$, $Y = 0$ and $L + T\sin\alpha = mg\cos\gamma$ with $\gamma = 0$, so that the angular dynamics become $\dot{\chi} = 0$ and $\dot{\gamma} = 0$. For notational convenience, we consider straight and level flight to be a (null) maneuver primitive, although few pilots would use this language. Conversely, a skid-to-turn maneuver can be achieved through choice of u_a, u_e, and u_r controls that achieve $\beta \neq 0$, $\sigma = 0$, $Y(u_r) \neq 0$ and $L + T\sin\alpha = mg\cos\gamma$, so that the angular dynamics become $\dot{\chi} = Y(u_r)\cos\beta$ and $\dot{\gamma} = 0$.

If we are provided with a set of usable maneuver primitives then we can consider control of the translational dynamics (5) to be a constrained control problem in which control inputs $(\dot{\chi}, \dot{\gamma})$ must be taken from a set of stable maneuver primitives. This constrained control design problem is conceptually much simpler than the unconstrained nonlinear control problem for the complete rigid-body dynamics (1)-(4), with the dual control objectives of achieving stable flight and satisfactory inspection performance.

C. Integrated Control System Design for Automated Inspection Aircraft

In aircraft systems, each sub-system is typically designed separately and then integrated together (with the possibility of some redesign to incrementally improve performance after integration). Alternatively, considering the design in an integrated way has the potential practical benefits of better system performance after fewer design iterations that more completely exploits the relationships between the subsystems [20].

Fig. 1 shows the three main aircraft control loops in our proposed approach. These loops correspond to the three sub-problems of the aircraft inspection control problem: trajectory planning, guidance, and maneuvering. The trajectory planning loop must determine a safe and efficient inspection trajectory for the aircraft and this function is shown in Fig. 1 as the receding virtual waypoint (RVWP) block. The guidance loop must determine acceleration commands that minimizes both the position and velocity vector mismatch between the aircraft and the inspection trajectory (this function is shown as the guidance block in Fig. 1). The maneuver selection block executes the maneuver primitive that achieves the guidance commands, so that the autopilot (shown as the autopilot block in Fig. 1) maintains aircraft body attitude so that infrastructure inspection can occur.

The absence of a human pilot in the control loop and the particular features of the aircraft inspection problem suggests that the three sub-problems should be considered in an integrated manner. Automatic control of air vehicles typically involves a guidance loop (typical bandwidth 1 Hz) that provides reference commands (e.g. acceleration commands expressed in body-coordinate frame) and an autopilot loop (typical bandwidth 50 Hz) that maintains the stability of the aircraft. These two loops (guidance and autopilot) correspond to different time scales in the aircraft dynamics [7], [20], [21], [23]. The main design benefit of this multi-loop structure is that it simplifies the design process because each loop can be separately designed. In our integrated design methodology, rather than consider each sub-system as an individual component with no connectivity to the others, the relationships between the sub-systems are exploited. Specifically, the RVWP trajectory planning approach can anticipate the upcoming changes in line direction which improves guidance loop effectiveness. The low-bandwidth guidance loop can then anticipate upcoming commands allowing reduction in autopilot response time requirements. The high-bandwidth autopilot loop can increase the effectiveness of the guidance loop.

Remark: Conversely, in the UAV control systems literature, there is often no clear guidance loop. Instead, autopilot loops appear to be be directly manipulated in a crude manner to achieve guidance objectives without a clear understanding of the coupling between slow guidance objectives and fast platform stabilisation issues (for examples, see [4], [5], [8], [24], [36]). This crude approach risks the introduction of unwanted instabilities and can make practical implementation more complex.

D. Implicit Trajectory Planning

Trajectory planning problems have been examined extensively in the literature by many authors [17], [18], [19], [22], [36]. Here we suggest that the infrastructure inspection trajectory can be implicitly described using receding virtual waypoints (RVWPs), where a RVWP is a waypoint that moves along the desired path at some distance d ahead of the aircraft as shown in Fig. 2 (also see [23]). These RVWPs can be introduced into the guidance loop as shown in Fig. 1. The RVWP approach allows the aircraft to track through changes in line direction. However it should be noted that the RVWP can impact the stability of the control loop due to the introduction of an extra feedback path. We shall assume that a RVWP approach to the trajectory planning sub-problem is appropriate. Although we discuss the trajectory planning problem and RVWP to explain our overall integrated design, we shall limit the rest of this paper's focus to the two remaining sub-problems: the guidance problem and the maneuver problem, to be examined in following Sections III and IV respectively.

III. Guidance and Inspection Planning

A. The Infrastructure under Inspection

Let us assume that infrastructure can be represented as a line in coordinate space of length L and let $\nu \in [0, L]$ be a uniform parameterisation variable so that $\bar{r}(\nu) = [\bar{x}(\nu), \bar{y}(\nu), \bar{z}(\nu)]$ is a parameterised description of location of the infrastructure under inspection. We assume that $\bar{x}(\nu)$, $\bar{y}(\nu)$ and $\bar{z}(\nu)$ are each C^0 continuous in ν so that $\nu \in [0, L]$ traces out the location of a continuous piece of infrastructure in coordinate space (with the possibility of step changes in line direction). An example of such an infrastructure asset is a power line.

During flight, the aircraft mounted camera used for inspection will experience rotation with respect to the basic navigation frame; this rotation is described by the Euler angles Θ. For all $\nu \in [0, L]$, we let $\psi^\nu(r)$, $\theta^\nu(r)$, $\phi^\nu(r)$ and $d^\nu(r)$ denote the pitch angle, yaw angle, roll angle and range from the camera (frame) mounted on the aircraft at location $r \in R^3$ to the infrastructure $\bar{r}(\nu)$. As shorthand, we let $\Theta^\nu(r) = [\psi^\nu(r), \theta^\nu(r), \phi^\nu(r), d^\nu(r)]$. Let S_{fov} denote the field-of-view of the camera in the sense that $\Theta^\nu(r) \in S_{fov}$ implies the infrastructure at ν can be inspected by the camera at location $r \in R^3$.

We now introduce two definitions:

Definition 3.1: If we consider an inspection path $r^n_{a,b}$, we say that inspection is **complete** when for each $\nu \in [0, L]$ there is some $t \in [a, b)$ such that $\Theta^\nu(r^n_t) \in S_{fov}$.

Definition 3.2: If we consider an inspection path $r^n_{a,b}$, we say that inspection has been **continuous** when for every $t \in [a, b)$ there is a $\nu \in [0, L]$ such that $\Theta^\nu(r^n_t) \in S_{fov}$.

Both complete and continuous inspection are desirable inspection characteristics. In fact, given an infrastructure asset $\bar{r}(\nu)$ we could state our infrastructure inspection problem as finding a control strategy for our dynamics that achieves complete inspection in the shortest period of time. Intuitively, we expect time-efficient inspection solutions to involve long periods of continuous inspection.

B. Guidance for Infrastructure Inspection

Let us assume that our infrastructure is piecewise linear, with minor direction changes in the sense of being well within the turning capabilities of our aircraft. Let us assume that there are no height variations in our infrastructure so that $\bar{z}(\nu) = \bar{z}$ for all $\nu \in [0, L]$. Let there be a pre-specific height h from which inspection is desirable. This means that a candidate inspection flight path is $\bar{r}^*(\nu) = [\bar{x}(\nu), \bar{y}(\nu), \bar{z} + h]$. The aircraft will not always be on this inspection path, but let us denote the closest point on our preferred inspection path to current aircraft location r_t^n to be $\nu^*(r_t^n)$ where

$$\nu^*(r_t^n) = \arg\min_{\nu} |r_t^n - \bar{r}^*(\nu)|. \tag{7}$$

Due to the nature of an aircraft's translational dynamics it is useful to introduce a waypoint that is located on the infrastructure. For an aircraft at location r_t^n a receding virtual waypoint $r^{wp}(r_t^n)$ with look-ahead distance d will be defined as

$$r^{wp}(r_t^n) = \bar{r_t^n}^*(\nu^*(r_t^n) + d) \tag{8}$$

and let $\tilde{r}(r_t^n) = r_t^n - r^{wp}(r_t^n)$ denote the tracking error from the receding virtual waypoint.

We now introduce an appropriate control problem. Let us assume that the autopilot dynamics are sufficiently fast so that $(\alpha, \beta, \sigma, L, T, D, Y)$ can be considered set-points for (6), achieving maneuver primitives with constant $(\dot{\chi}, \dot{\gamma})$. We let $\bar{u}_t$ denote the set-points or the maneuver primitives $(\dot{\chi}, \dot{\gamma})$ that are active at time t and let $M(r)$ denote the set of candidate maneuver primitives (with stable flight and $\Theta^\nu(r_t^n) \in S_{fov}$). Hence $\bar{u}_t \in M(r_t^n)$ will denote a control corresponding to a maneuver primitive that has stable flight and allows inspection from location r_t^n.

Then we can define the **optimal receding virtual waypoint guidance problem** as finding a total inspection time T and control $\bar{u}_{0,T}$, where $\bar{u}_t \in M(r_t^n(\bar{u}_{0,t}))$ for all $t \in [0, T)$, that minimises

$$J(\bar{u}_{0,T}, T) = \int_0^T \tilde{r}(r_t^n(\bar{u}_{0,t}))^2 + \dot{\tilde{r}}(r_t^n(\bar{u}_{0,t}))^2 dt \tag{9}$$

and achieves complete inspection. The importance of this cost function is established in the following lemma.

Lemma 3.1: Assume the infrastructure $\bar{r}^*(\nu)$ is linear and assume the receding virtual waypoint $r^{wp}(r_t^n)$ has fixed look-ahead d for aircraft dynamics (5). The minimum of (9) occurs at $\tilde{r} = d$ and $\dot{\tilde{r}} = 0$, and this corresponds to a tracking inspection aircraft in the sense that the tracking conditions $r_t^n = \bar{r}(\nu^*(r_t^n))$ and $\dot{r}_t^n = \dot{\bar{r}}(\nu^*(r_t^n))$ hold.

Proof: First we note that $\tilde{r} = d$ and $\dot{\tilde{r}} = 0$ is the unconstrained minimum of (9), and that valid dynamics (5) at this minimum exist (that is, flight corresponding to $r_t^n = \bar{r_t^n}^*(\nu^*(r_t^n))$ is possible). To show the tracking condition holds we note that $\tilde{r}(r_t^n) = r_t^n - r^{wp}(r_t^n)$, and hence in the above flight condition $\dot{\tilde{r}} = \dot{r}_t^n - \dot{r}^{wp}(r_t^n) = \dot{r}_t^n - \dot{\bar{r}_t^n}^*(\nu^*(r_t^n)) = 0$. ■

Lemma 3.1 shows that the objective of the optimal receding virtual waypoint guidance problem is to achieve complete inspection in the shortest time whilst minimising the tracking error.

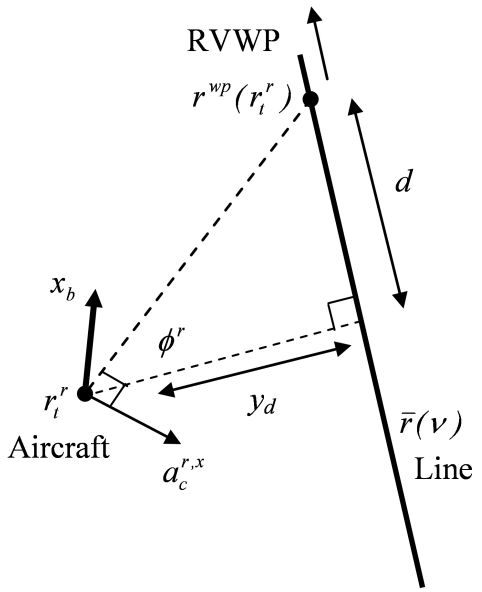

Fig. 2. Relative inspection dynamics with a receding virtual waypoint.

C. Guidance in the Infrastructure frame

We now consider dynamics in a coordinate system attached to the infrastructure so that the origin of this system is at $\bar{r}(0)$ and the positive y-axis points along the infrastructure. We use the superscript r to denote quantities in this system. Let us assume level inspection flight so that $\gamma = 0$, $\dot{\gamma} = 0$ and $z^n = \bar{z} + h$, then in this infrastructure frame the aircraft dynamics can be expressed as

$$\begin{aligned} \dot{x}^r &= V \cos\chi^r \\ \dot{y}^r &= V \sin\chi^r. \end{aligned} \tag{10}$$

In this infrastructure coordinate system, we let $\tilde{r}_t^r = r_t^r - r^{wp}(r_t^r)$ denote the relative dynamics. For a waypoint with a fixed look-ahead distance d (also see Remark 1 below), we can write the dynamics relative to the waypoint as

$$\begin{aligned} \dot{\tilde{x}}^r &= V \cos\chi^r \\ \dot{\tilde{y}}^r &= 0. \end{aligned} \tag{11}$$

This description allows us to re-pose the optimal receding virtual waypoint guidance problem as an optimal control problem with cost (9) on dynamics (11), with the state-based control constraint $u \in \tilde{M}(\tilde{x})$, where $\tilde{M}(.)$ is a re-expression of inspection constraints $M(.)$ in terms of the relative dynamics. We highlight that the conclusions of Lemma 3.1 still hold because achieving $\tilde{r}^r = 0$ and $\dot{\tilde{r}}^r = 0$ implies $\tilde{r} = d$ and $\dot{\tilde{r}} = 0$.

Due to the reduced state dimension, the constrained non-linear optimal control problem posed on (11) can be solved using numeric based dynamic programming approaches such as the Markov Chain technique [37]. An example of these approximation techniques applied to optimal guidance problems is provided in [38].

To further simplify our control design problem, let us consider the RVWP with varying look-ahead distance $d =$

$x^r \tan\phi^r$ where ϕ^r is the desired angle at which we wish to approach the infrastructure. This is the situation shown in Fig. 2, where the cross-track error, $y_d = \tilde{x}^r$, is also indicated on the figure. We can write the relative dynamics with look-ahead distance $d = x^r \tan\phi^r$ as

$$\begin{aligned} \dot{\tilde{x}}^r &= V\cos\chi^r \\ \dot{\tilde{y}}^r &= V\cos\chi^r \tan\phi^r. \end{aligned} \tag{12}$$

Lemma 3.2: Assume that we choose the desired approach angle ϕ^r to match the current course angle in the sense that $\tan\phi^r = \tan\chi^r$, then under small $\dot{\chi}^r$ and χ^r assumptions the relative dynamics can be approximated as

$$\begin{aligned} \dot{\tilde{x}}^r &= V\cos\chi^r \\ \dot{\tilde{y}}^r &= V\sin\chi^r. \end{aligned} \tag{13}$$

Moreover, under small angle approximations, the unconstrained optimal inspection law for cost $J(u_{0,T}) = \tilde{r}(r_T^r(\bar{u}_{0,T}))^2 + \dot{\tilde{r}}(r_T^r(\bar{u}_{0,T}))^2$ can be represented as

$$a_{c,PG}^{r,x} = V_c(4\dot{\lambda} + 2(\lambda - \overline{\lambda})/t_{go}), \tag{14}$$

where $a_{c,PG}^{r,x}$ is the commanded acceleration (expressed as feedback in λ and t_{go}), V_c is the closing velocity, $\lambda = \tan^{-1}(\tilde{y}^r/\tilde{x}^r)$ is the line-of-sight angle and $t_{go} = |\tilde{r}^r|/V$ is the time-to-go. Here, $\overline{\lambda}$ is the direction of the line to be inspected (also see Remark 2 below).

Proof: Suitably small $\dot{\chi}^r$ allows approximation of $\dot{d} = \dot{\tilde{x}}^r \tan\phi^r + \frac{d}{dt}\{\tan\phi^r\} \approx \dot{\tilde{x}}^r \tan\phi^r$. The relative dynamics (13) then follow from simple trigonometry applied to (12). Once (13) is established, the proofs of [30] or [32] show that the small χ^r angle approximations lead to the lemma result. ■

Remarks:

1) The choice of look ahead distance d impacts the closed-loop stability of the guidance loop as confirmed by our simulation and flight testing efforts. Long d corresponds to conservative action, whilst short d corresponds to rapid response.
2) Note that in the coordinate system used here $\overline{\lambda} = 0$ but we often implement (14) in a navigation frame and $\overline{\lambda}$ will be equal to the heading of the infrastructure under inspection.

IV. Adaptive Maneuver Selection

The aircraft maneuver dynamics used to track the inspected linear infrastructure have an important role in maintaining inspection. For example, there is often a requirement for body-fixed downward-looking cameras to capture the objects on the ground within their fixed and limited field of view [4], [5], [7], [8], [16], [17]. For non-gimballed cameras aircraft roll is a particularly important issue, but minimizing the roll motion assists gimballed systems as well. For these reasons, we consider the idea of selecting or combining maneuvers to achieve the translational requirements of the guidance module whilst ensuring that $\Theta_t^\nu \in S_{fov}$ for all flight. In this study, we consider bank-to-turn (BTT), skid-to-turn (STT) and constrained bank-to-turn (CBTT) maneuvers and adaptive mixtures of these maneuvers.

A. Pure Maneuvers

A pure BTT maneuver involves the aircraft banking (rolling) and is the typical way a fixed-wing aircraft achieves a change of heading, or commanded lateral acceleration [27]. A body-fixed frame lateral acceleration $a_c^{y,b}$ can be achieved by commanding the roll angle ϕ_c [16], [33]

$$\phi_c = \tan^{-1}\left(\frac{a_c^{y,b}}{g}\right), \tag{15}$$

where that u_a, u_e, and u_r are chosen so that $\beta = 0$, $Y = 0$ and also to ensure steady flight in the sense that $(L + T\sin\alpha)\cos\sigma = mg\cos\gamma$. Substitution in (6) shows that a BTT maneuver can be described by the dynamics

$$\begin{aligned} \dot{\chi} &= \frac{g}{V}\tan\sigma \\ \dot{\phi} &= P_{roll}(\phi_c - \phi) \\ \dot{\gamma} &= 0 \\ \sigma &= \cos^{-1}\left(\frac{\cos\alpha\cos\theta\cos\phi + \sin\alpha\sin\theta}{\cos\gamma}\right) \end{aligned} \tag{16}$$

where P_{roll} provides a first order approximation of the autopilot's lower-level roll loop.

A pure STT maneuver is an alternative way of changing heading that does not involve rolling the aircraft, but rather involves moving the aircraft nose sidewards relative to the velocity vector [17]. For a pure STT maneuver with acceleration $a_c^{y,b}$, the controls u_a, u_e, and u_r should be set to achieve $\beta \neq 0$, $\sigma = 0$ and $Y(u_r)\cos\beta = m\cos(\gamma)a_c^{y,b}$ and to achieve steady state flight in the sense that $L + T\sin\alpha = mg\cos\gamma$. We can use kinematic considerations and knowledge that the centripetal acceleration $\dot{\chi} = \frac{a_c^{y,b}}{V}$ to derive the dynamics for the STT maneuver,

$$\begin{aligned} \dot{\chi} &= \frac{Y(u_r)\cos\beta}{Vm\cos\gamma} \\ \dot{\phi} &= 0 \\ \dot{\gamma} &= 0, \end{aligned} \tag{17}$$

where the dynamics of (6) implies that to achieve a STT maneuver as described, the condition $Y\sin\beta = mg\sin\gamma$ must also hold. We highlight that only a small side-force $Y(u_r)$ can be produced due to the dynamic limitations of typical fixed-wing aircraft and hence STT is not suitable for large maneuvers.

As the name suggests, a CBTT maneuver is a BTT maneuver in which the range of commanded bank angle has been constrained. The dynamics of a CBTT maneuver are also described by (16), but with a commanded roll angle

$$\phi_c = \begin{cases} \tan^{-1}\left(\frac{a_c^{y,b}}{g}\right) & \text{if } |a_c^{y,b}| \leq g\tan(\phi_{max}) \\ sign(a_c^{y,b})\phi_{max} & \text{otherwise} \end{cases} \tag{18}$$

where $\phi_{max} \geq 0$ is the maximum bank angle that can be commanded by the CBTT maneuver. Note that a CBTT maneuver may not fully achieve the commanded acceleration because of the bank angle constraint.

B. Adaptive and Hybrid Maneuvers

In this section, we investigate several adaptive maneuver selection approaches in which the maneuver dynamics used by the aircraft can change during the inspection mission to improve attitude performance of the aircraft.

The simplest adaptive maneuver strategy involves pure switching between STT and BTT maneuvers. Let a_{STT} denote the acceleration threshold used for switching between STT and BTT maneuvers. The dynamics of a pure STT/BTT maneuver switching strategy can be expressed as [28], [29]:

$$\begin{cases} \dot{\chi} = \frac{Y^S(u_r)\cos\beta}{Vm\cos\gamma} \\ \dot{\phi} = 0 \\ \dot{\gamma} = 0 \end{cases} \quad \text{if } \left|a_c^{y,b}\right| < a_{STT}$$
$$\begin{cases} \dot{\chi} = \frac{g}{V}\tan\sigma \\ \dot{\phi} = P_{roll}\left(\phi_c - \phi\right) \\ \dot{\gamma} = 0 \\ \sigma = \cos^{-1}\left(\frac{\cos\alpha\cos\theta\cos\phi + \sin\alpha\sin\theta}{\cos\gamma}\right) \end{cases} \quad \text{otherwise} \tag{19}$$

where ϕ_c is given by (15) and the rudder control u_r has been used to set $Y^S(u_r)\cos(\beta) = m\cos(\gamma)a_c^{y,b}$.

Alternatively, a possible hybrid approach involves a mixture of BTT and STT maneuvers [28], [29]. Let $\gamma_S(.)$ denote some blending function that represents the proportion of commanded acceleration $a_c^{y,b}$ to be supplied by the STT component of the hybrid maneuver. Then we let $\phi_c^\gamma = \tan^{-1}((1-\gamma_S)a_c^{y,b}/g)$ denote the roll angle for the BTT component of the maneuver. From the kinematic considerations we can see that to perform this maneuver, the controls u_a, u_e, and u_r should be set to achieve $\beta \neq 0$, $\sigma \neq 0$, $Y \neq 0$ (and to achieve steady flight in the sense that $(L + T\sin\alpha)\cos\sigma = mg\cos\gamma$). Following this analysis a mixed STT/BTT maneuver can be described by the dynamics

$$\begin{aligned} \dot{\chi} &= \tfrac{g}{V}\tan\sigma + \tfrac{Y^{SB}(u_r)\cos\beta}{Vm\cos\gamma} \\ \dot{\phi} &= P_{roll}\left(\phi_c^\gamma - \phi\right) \\ \dot{\gamma} &= 0 \\ \sigma &= \cos^{-1}\left(\tfrac{\cos\alpha\cos\theta\cos\phi + \sin\alpha\sin\theta}{\cos\gamma}\right) \end{aligned} \tag{20}$$

where the rudder control u_r and aileron control u_a has been used to set $Y^{SB}(u_r)\cos(\beta)\cos(\sigma(u_a)) = \gamma_S m\cos(\gamma)a_c^{y,b}$.

We highlight that this mixed STT/BTT maneuver (involving a pure BTT maneuver plus a pure STT maneuver) can also be derived from the dynamics (6) by making small α, β, γ and σ angle assumptions and also with the assumption of steady flight (constant velocity and $\dot{\gamma} = 0$). Again note that the bank angle σ is related to roll angle ϕ through the expression $\cos\sigma\cos\gamma = \cos\alpha\cos\theta\cos\phi + \sin\alpha\sin\theta$ [35] which reduces to $\sigma \approx \phi$ for small α, θ, γ angles.

Our desire to improve inspection performance motivates the proposal of a new adaptive maneuver selection approach involving a mixture of STT and CBTT maneuvers. The idea of this new mixture is to ensure the aircraft roll angle is constrained less than ϕ_{max} but also to minimise an associated reduction in line tracking performance due to possible unfulfilled acceleration with a pure CBTT maneuver. This is achieved by supplementing a CBTT maneuver with a STT maneuver when the pure CBTT fails to deliver all acceleration commanded by the guidance law. Under the same assumptions made for (20) the dynamics of the mixed STT/CBTT maneuver can be expressed as

$$\begin{aligned} \dot{\chi} &= \tfrac{g}{V}\tan\sigma + \tfrac{Y^{SC}(u_r)\cos\beta}{Vm\cos\gamma} \\ \dot{\phi} &= P_{roll}\left(\phi_c - \phi\right) \\ \dot{\gamma} &= 0 \end{aligned} \tag{21}$$

where $\phi_c \leq \phi_{max}$ as given by (18), and

$$Y^{SC}(u_r)\cos(\beta)\cos\sigma = m\cos(\gamma)(a_c^{y,b} - g\tan\phi_{max})$$

provides the compensating STT component of the maneuver when the roll constraint is active. It should be noted, that the compensating STT maneuver combined with the CBTT maneuver may not fully achieve the commanded acceleration, depending upon the characteristics of the platform. In later simulation studies, this adaptive maneuver approach will be shown to improve inspection performance by avoiding large roll angles [8], [17].

V. Simulation Studies and Experimental Flight Tests

To study the performance of the proposed guidance and adaptive maneuver approaches in simulation, the complete control architecture as described in Fig. 1 was implemented in MATLAB. The dynamics under simulation consisted of full six degree-of-freedom nonlinear semi-coupled equations of motion with rigid-body, fixed mass, uniform gravity and nil wind assumptions [39]. We highlight that the aircraft dynamics used in our simulations had higher fidelity than those we used for designing the guidance law. Therefore the following results contain violations of steady flight assumptions (velocity non-constant, non-zero $\dot{\gamma}$) and coupling between longitudinal and lateral motion as typical in realistic flying conditions. This provides some illustration of the robustness of our design process.

The platform aerodynamics considered was the Navion model from Unmanned Dynamic's Aerosim Blockset for Simulink, which is a single engine aircraft of approximately 10 m wingspan and 1000 kg weight. Full autopilot dynamics were simulated and the autopilot loops, which included standard PID control, were tuned for aircraft stability only once, and unchanged for all simulations. The autopilot attitude and velocity loops were set to maintain a constant altitude and velocity of 133 m and 30 m/s, respectively. Maximum bounds were set on commanded course angle rates $\dot{\chi}_c$ and bank angles ϕ_c of $11.5^\circ/s$ and 40°, respectively, to ensure rejection of any unrealistic commands [4], [5]. The sample period used in simulating aircraft motion was 0.02 s, leading to a distance resolution of approximately 0.6 m in our simulation environment.

In addition to using MATLAB simulations, we have also simulated the overall performance of the guidance and RVWP tracking algorithms in X-plane [40] and numerous experimental flight tests on a Cessna 172 aircraft have been conducted. In the following sections, we first study PG law sensitivity against

three other candidate guidance approaches in SectionV-A. We then evaluate overall performance by presenting results from experimental flight testing in Section V-B. We finally examine the performance of our proposed hybrid maneuver strategy in Section V-C.

A. Guidance Simulation Studies

The benefits of the proposed PG law were studied against three other candidate guidance approaches using the MATLAB simulation environment. The first alternative was the proportional navigation (PN) guidance law which has been studied extensively in the missile guidance community [31]. The PN law is defined through the acceleration command $a^{r,x}_{c,PN}$:

$$a^{r,x}_{c,PN} = V_c N \dot{\lambda} \tag{22}$$

where $N = 3$ is the navigation gain [31].

The second alternative considered was a biased PN law (BPN) which is proposed in [7], [16] for the infrastructure tracking problem. The BPN law is defined through the acceleration command $a^{r,x}_{c,BPN}$:

$$a^{r,x}_{c,BPN} = V_c N \dot{\lambda} + L\,|y_d|\,sign(y_d) \tag{23}$$

where L is a gain that needs to be tuned.

The third and final alternative we considered was Frew's nonlinear arctan controller proposed in [4]. This guidance law is defined by the equation,

$$\dot{\psi} = P_{AT}\left[\tan^{-1}\left(\frac{\dot{x}^r}{\sqrt{V^2_{IAS} - \dot{x}^r}}\right) - \tan^{-1}\left(\frac{-x^r}{d}\right)\right] \tag{24}$$

where P_{AT} is a tuned proportional gain and V_{IAS} is the indicated airspeed.

The performance of the different guidance laws were compared in terms of both cross-track and heading error. For all the studies that follow, the BPN guidance law with $L = 0.05$ was found to give good performance. Frew's arctan controller P_{AT} was also tuned for good performance. We begin by examining the sensitivity of the four guidance laws to initial waypoint distance and initial heading. The set of candidate maneuvers $M(\cdot)$ available to each guidance law was limited to BTT maneuvers.

1) Impact of Initial Waypoint Distance Variations, with Initial Heading Fixed: This MATLAB simulation study evaluated the sensitivity of the four guidance laws to variation in initial distance to a fixed waypoint. This study was performed by simulated guided flight from point P to fixed waypoint WP_n at an initial distance ahead of d_n and initial heading angle of θ_n, as shown in Fig. 3. The test was repeated for a number of increasing initial distances from 125-1350 m in 25 m increments with both initial heading θ_n and desired heading at the waypoint fixed at 10°.

The cross-track error results are shown in Fig. 4, plotted against the distances d to the waypoint. For the shortest d of 125 m the PG law gave smallest y_d, however as d increased the cross-track error of the PG law was up to 8 m worse than PN or BPN for distance ahead d of between 200-500 m. As seen, for most d values Frew's arctan controller tended to exhibit

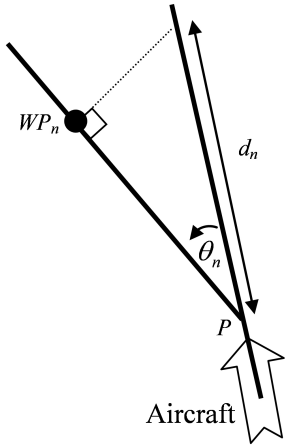

Fig. 3. Influence of initial distance and heading angle to fixed waypoint.

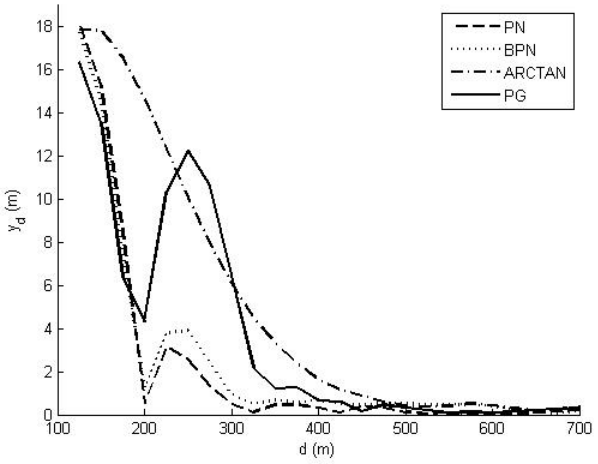

Fig. 4. Cross-track errors under variation of initial waypoint distance.

greater error than the other guidance laws. For d greater than 500 m, all laws gave similar cross-track error performance.

The intercept heading angle error $\Delta\theta$ results are shown in Fig. 5, plotted against d. Intercept heading angle error $\Delta\theta$ was defined as the difference between the aircraft heading angle ψ and desired heading θ. The arctan controller gave the smallest heading error $\Delta\theta$ for d between 125-280 m whilst the PG and BPN laws gave the smaller angle error $\Delta\theta$ for d values greater than 400 m. The PN law angle error was consistently larger than the other PN-based laws for most values of d. This occurred because the PN law does not have any explicit control over the intercept angle at the waypoint. The BPN and PG laws gave comparable performance particularly for $d \leq 500$ m. Despite the BPN law having no explicit impact angle requirement, a heading requirement is implicit in the bias term involving y_d. However, good performance of the BPN as was shown here was dependent upon good tuning of the law, in which case a poorly tuned BPN law would not have performed as well (see Remark 1 below).

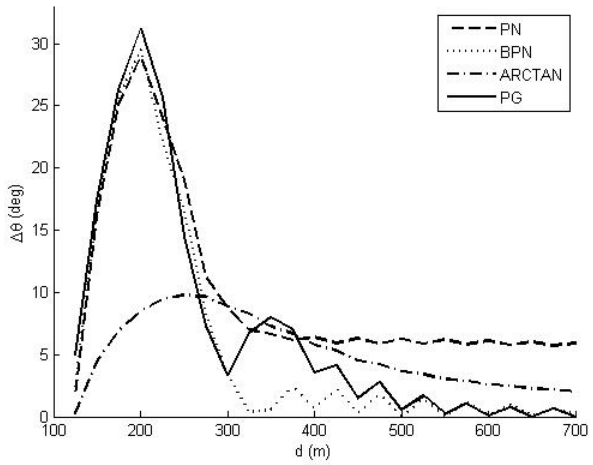

Fig. 5. Heading errors under variation of initial waypoint distance.

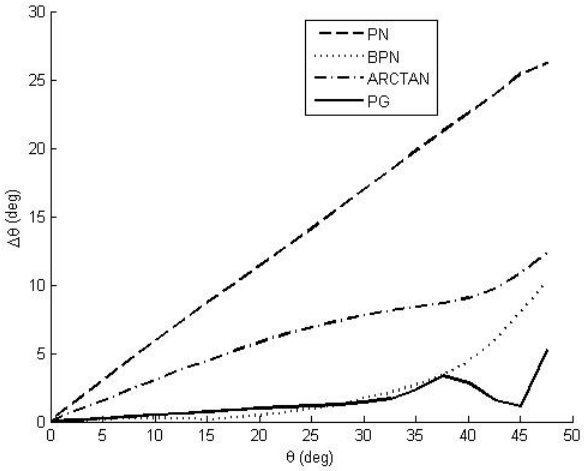

Fig. 7. Heading errors under variation of initial heading angle.

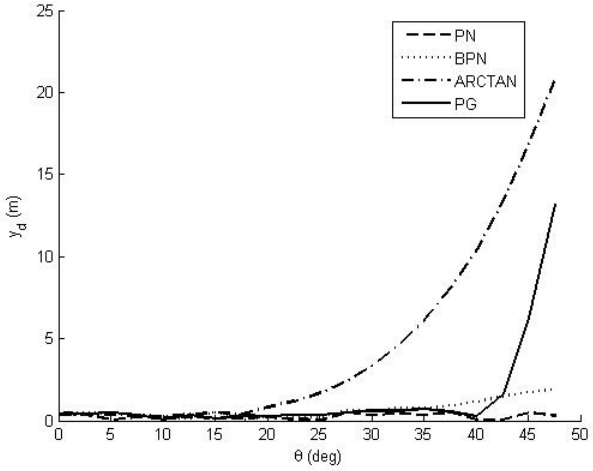

Fig. 6. Cross-track errors under variation of initial heading angle.

2) Impact of Initial Heading Variations, with Initial Waypoint Distance Fixed: This MATLAB simulation study evaluated the sensitivity of the four guidance laws to initial heading angle to a fixed waypoint. This study involved simulation of guided flight from point P to fixed waypoint WP_n as shown in Fig. 3. The test was repeated for a number of increasing initial heading angles θ_n from 0° to 47.5° in 2.5° increments, with a fixed look-ahead distance d_n of 700 m.

The cross-track error results for different initial heading angles θ are shown in Fig. 6. As seen there was no significant difference observed between the cross-track error of the laws for initial heading angle θ between 0° and 17°. For initial angles greater than 17° the error increased exponentially for the arctan controller. The cross-track error started to increase slowly for BPN with initial angles greater than 35°, and increased for the PG law for initial angles greater than 42°.

Fig. 7 plots the intercept heading error $\Delta\theta$ against initial heading θ. As seen, the intercept heading error increased near-linearly with initial heading angle θ for PN and arctan. The BPN and PG laws exhibited smallest intercept heading error with increasing initial heading angle θ for $\theta \leq 37^\circ$. At higher initial heading angles the controllers gave larger error because these angles violated the small angle assumptions used in developing these guidance laws.

3) Sensitivity to Wind: In MATLAB we repeated the previous tests for a range of simulated wind conditions and similar cross-track errors were seen, except for a drift angle in the heading error results. This demonstrated insensitivity to wind and this was also confirmed by later experimental flight tests and simulation studies in an X-Plane simulation environment.

4) Summary: For the initial distance and initial heading angle to waypoint studies (with fixed waypoints), the PN exhibited good cross-track error performance but with poor intercept heading angle error performance. The BPN law exhibited good cross-track and heading angle error performance, but is dependent upon a suitable value of L being determined. Frew's arctan controller exhibited poor cross-track error and heading angle error. The PG law exhibited reasonable cross-track error performance, and reasonable heading angle error performance.

B. Experimental Flight Tests Above Kingaroy Power-line Test Region (South-East Queensland, Australia)

In this section we present results from experimental flight testing of guidance laws with RVWP-based tracking, above a 10 km length of power-line in Kingaroy, Queensland, Australia. The flight test platform was a Cessna 172 aircraft equipped with roll-steer capable KAP140 autopilot and Novatel SPAN integrated GPS/INS. Guidance commands were sent at 1 Hz to the autopilot as roll commands. That is, the set of candidate maneuvers $M(\cdot)$ available to each guidance law under study was limited to BTT-type maneuvers (further details are provided below).

Guidance law performance with RVWP tracking was first tested extensively in an X-plane simulation environment [40] which was designed to match the performance of the Cessna 172. These tests led to the following two practical PG law design implementation choices being incorporated:

1) Rather than using aircraft ground velocity V as closing velocity in the precision guidance law (14), it was found that setting $V_c = V_{ac} - 0.5V_{rvwp}$ where V_{ac} and V_{rvwp} are ground velocities of the aircraft and RVWP respectively, provided improved flight stability characteristics.
2) It was necessary to add a lag compensator in the form of a PID loop around the PG law to mitigate an aircraft time constant of 6.5 seconds.

Numerous flight tests were then conducted to confirm guidance law performance. Here, we present the results of three flight tests that compare the performance of a pure pursuit (PP) guidance law (similar to arctan law) with a RVWP look-ahead distance of 1000 m, a PG law with a RVWP with look ahead distance of 1000 m and a PG law with a RVWP with look ahead distance of 700 m.

The pure pursuit guidance law is:

$$\dot{\psi} = k_p(\psi_d - \psi_a) \tag{25}$$

where $\psi_d = \overline{\lambda}$ is the desired heading of the power line, ψ_a is the current aircraft heading and k_p is a tunable gain. The arctan law could not be flown because airspeed measurements were not available in the test aircraft.

Flight test conditions were as follows:

1) Wind conditions were 15 knots South West with low-moderate turbulence.
2) Speed and altitude was kept under manual pilot control during the tests, with average ground speed of 46 m/s and average altitude of 1500 ft.
3) Aircraft rudder was kept in the neutral position and altitude and airspeed attempted to be kept constant via manual pilot control.
4) Roll angle was constrained to approximately 15 deg which was the turn-rate limit of the autopilot.

Fig. 8 shows the ground track of the aircraft (in white) over the power line (in black) for the PG 700 m flight test. Cross-track and angle error results are summarised in Table I. This table shows that the performance of the PG 1000 m approach gave approximately 20 m smaller average cross track error and 1 deg smaller angle error than the pure pursuit (PP 1000 m). Shortening the RVWP look ahead distance to 700 m resulted in further reductions in cross-track and heading errors. However it should be noted that if the RVWP look ahead distance was set too short (say 500 m or less), this resulted in decreased stability in cross-track performance. This series of flight tests demonstrates that our integrated design featuring our proposed guidance law with RVWP trajectory planning can allow a standard aircraft autopilot (without any special tuning for this application of tracking power lines) to achieve good line-tracking performance. This leads to a more effective and lower-cost control system without requiring costly modification of the inner workings of the autopilot or control surfaces of the inspection aircraft.

1) Summary: Experimental flight tests over power lines at Kingaroy of the PG law with the RVWP tracking technique demonstrated that the PG law can give improved cross-track and heading error performance for power line tracking, compared to a pure pursuit (similar to arctan) guidance law.

Fig. 8. Plot of aircraft ground track (white) over Kingaroy power lines (black).

TABLE I
AVERAGE AND MAXIMUM CROSS-TRACK ERROR y_d AND INTERCEPT TRACK ANGLE ERROR $\Delta\theta$ FOR KINGAROY FLIGHT TESTS

	y_d avg (m)	y_d max (m)	$\Delta\theta$ avg (°)	$\Delta\theta$ max (°)
PG 700 m	14	187	3.6	34.7
PG 1000 m	35	181	4.4	41.2
PP 1000 m	56	245	5.5	45.6

C. Adaptive Maneuver Simulation Studies

These next MATLAB simulation studies illustrate the benefits of adaptive maneuver selection for infrastructure inspection.

1) Illustration of Mixed STT/CBTT Adaptive Maneuvers: To illustrate the mixed STT/CBTT adaptive maneuver selection, a simulation was made of an aircraft tracking a series of contiguous line segments using the mixed STT/CBTT adaptive maneuver and the PG law, with a RVWP set a fixed distance ahead on the line of $d = 150\ m$ (short look-ahead distance to emphasise turning requirements). From the aircraft's perspective, the line direction was initially straight ahead, then changed direction $10°$ to the left, then $20°$ to the right (see Fig. 9). A ϕ_{max} constraint of $10°$ was engaged and disengaged at 120s and 160s, respectively, and these two locations are indicated on Fig. 9 by the two square symbols. Outside this period the roll angle constraint was relaxed to $60°$ and allowed unconstrained flight.

Fig. 10 plots the cross-track error y_d and roll attitude angle ϕ of the aircraft with time. The sequence of ϕ_{max} changes is also shown. Initially, cross-track error y_d was approximately zero as the aircraft flew directly above the first line segment. After encountering the $10°$ change in line direction there was an increase in y_d as the aircraft "cut across the corner" of the two contiguous line segments. This behaviour is a feature of our RVWP tracking strategy and is highlighted in Fig. 9 which shows the behaviour at the corners (also see remark 2 below).

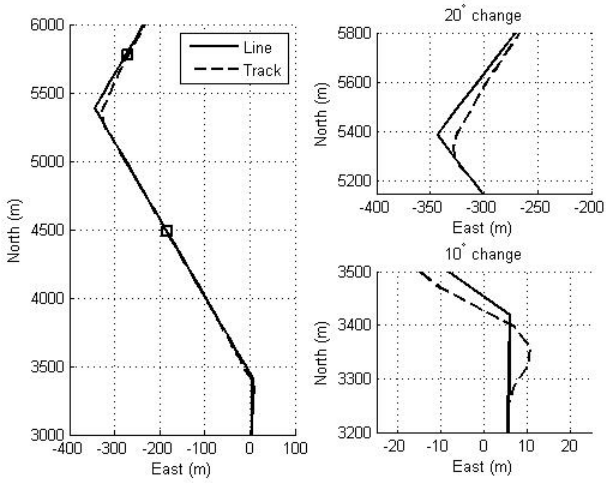

Fig. 9. Illustration of mixed STT/CBTT inspection trajectory behaviour. The points marked by the square symbol denote the start and end points of the $\phi_{max} = 10°$ constraint. Outside this line segment $\phi_{max} = 60°$.

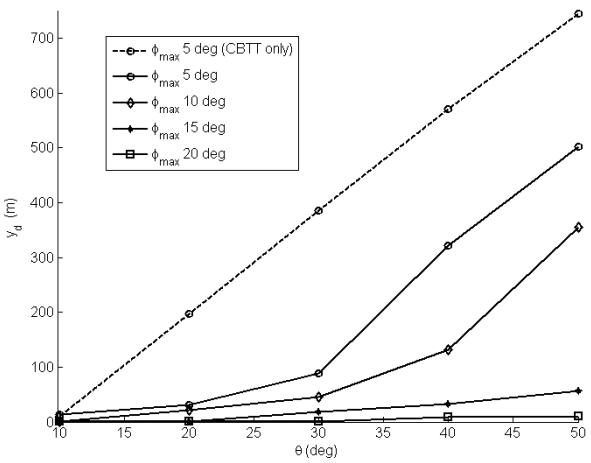

Fig. 11. Cross-track errors in mixed STT/CBTT approach for changes in maximum roll constraint ϕ_{max}, for different initial heading angle. A CBTT only case is also shown to compare the effect of not including a STT component.

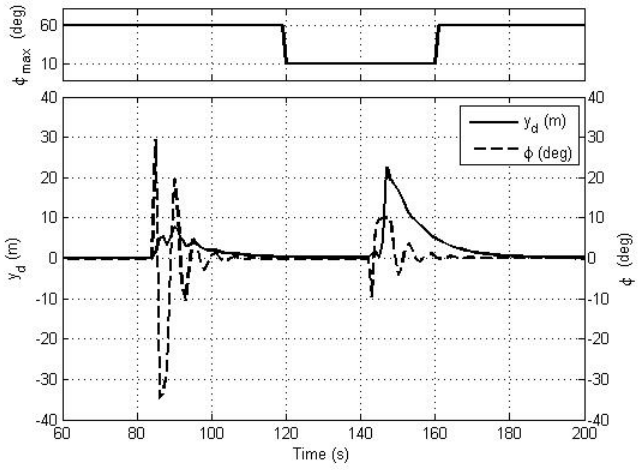

Fig. 10. Cross-track and heading errors exhibited by mixed STT/CBTT configuration during a period of active roll constraint.

As shown in Fig. 10 an aircraft roll angle of up to 30° was observed between 80-100 s as the aircraft rolled to align heading angle with the next line segment. At the second corner, under the $\phi_{max} = 10°$ constraint, we see a different trade-off between roll angle ($\leq 10°$) and cross-track error (out to a maximum of approximately 20 m).

2) Roll Constraints and Cross-track Error: The purpose of this test was to examine the impact of roll angle constraints on guidance with mixed STT/CBTT adaptive maneuvers. This guidance and maneuver combination was simulated in a manner similar to the earlier initial heading angle study (Section V-A2) but with d of 1000 m and velocity of 40 m/s. The BPN law was chosen for the guidance. The range of θ values considered were between $10°$ and $50°$ with maximum roll constraints $\phi_{max} \in \{5°, 10°, 15°, 20°\}$.

Fig. 11 plots cross-track error y_d against initial heading angle θ for different values of maximum roll constraint ϕ_{max} for the mixed STT/CBTT maneuver approach. A result for a CBTT without STT (CBTT only) maneuver is also given to show the benefit of using the STT to reduce unfulfilled accelerations, for $\phi_{max} = 5°$. A trade-off between roll constraints and cross-track error can be clearly seen. For increasing values of θ and decreasing ϕ_{max} there was increasing y_d error due to unfulfilled accelerations (also see Remark 3 below). This justifies our inclusion of a STT maneuver to reduce this increase in cross-track error by minimising unfulfilled accelerations. Comparing the two $\phi_{max} = 5°$ cases, a clear improvement in cross-track track error can be seen by inclusion of the STT component (compare a cross-track error of 400 m for the $\phi_{max} = 5°$ CBTT case but an improved cross-track error of 100 m for the $\phi_{max} = 5°$ STT/CBTT case at $\theta = 30°$). Improvements of STT/CBTT over CBTT were also seen for the other ϕ_{max} values (but lesser improvements were observed since CBTT behaviour approaches a pure BTT as ϕ_{max} increases). This illustrates that the inclusion of the STT component in a mixed STT/CBTT maneuver approach is effective in partially fulfilling the accelerations which cannot be achieved by a pure CBTT. Note that there was always an increase in cross-track error y_d with increasing initial heading angle θ (clearly seen in the $\phi_{max} = 5°$ and $\phi_{max} = 10°$ cases) because the amount of acceleration which the STT maneuver could produce was limited (due to fixed-wing aircraft dynamic limitations).

3) Summary: Our adaptive STT/CBTT maneuver study has shown the benefits of including a mixed hybrid STT/CBTT mode in the inspection application. Our proposed adaptive maneuver approach constrained the roll angle to within the desired constraint of $10°$ during a period of inspection. A second study illustrated the trade-off between achievable roll constraints and cross-track error with changes in initial heading angle. These results could be used as an initial estimate of inspection performance for certain desired roll constraints.

Remarks:

1) It was found through trial and error that for L values

too large (say ≥ 0.2), the BPN exhibited increasing instability with increasing L and the PG law typically outperformed it. For L values too small (say ≤ 0.01), the BPN behaviour approached the behaviour of PN, as might be expected.

2) Future research will investigate corner turning strategies, such as determination of d and placement of waypoints.
3) For larger ϕ_{max} values of 22.5° and above (not shown on Fig. 11), the behaviour approached that seen by a pure BTT (little or nil increase in cross-track error y_d with initial heading error θ), as might be expected.

VI. Conclusion

The first contribution of this paper was the proposal of a precision guidance law for guiding an aircraft to track linear infrastructure in a manner that maintained desirable position and orientation properties. The second contribution was the proposal of an adaptive maneuver selection approach, in which maneuvers were adaptively selected for improving the aircraft's attitude behaviour. The third contribution of this paper was to propose an integrated system design for the three standard sub-problems of trajectory planning, guidance and maneuvering. Simulation studies and flight tests illustrated the effectiveness of the proposed guidance law through comparison with other guidance laws. Finally, the adaptive maneuver approach was illustrated in simulation to improve roll motion behavior.

Acknowledgment

This work was conducted within the CRC for Spatial Information, established and supported under the Australian Government's Cooperative Research Centres Programme, and in conjunction with the Australian Research Centre for Aerospace Automation (ARCAA).

We acknowledge the efforts and assistance of Ryan Fechney in software development and testing for our simulation and flight testing activities.

References

[1] H. Madjidi, S. Negahdaripour and E. Bandari, "Vision-based positioning and terrain mapping by global alignment for UAVs", *Proc. IEEE Conf. Adv. Video Signal Based Surveillance, pp. 305-312*, 2003.

[2] D.B. Barber, J.D. Redding, T.W. McLain, R.W. Beard and C.N. Taylor, "Vision-based Geo-location using a Fixed-wing Miniature Air Vehicle", *Journal of Intelligent Robot Systems*, 47: 361-382, 2006.

[3] A. Gurtner, D.G. Greer, R. Glassock, L. Mejias, R.A. Walker and W.W. Boles, "Investigation of fish-eye lenses for small-UAV aerial photography", *IEEE Transactions on Geoscience and Remote Sensing, 47(3). pp. 709-721.*, 2009.

[4] E. Frew, T. McGee, Z. Kim, X. Xiao, S. Jackson, M. Morimoto, S. Rathinam, J. Padial and R. Sengupta, "Vision-Based Road-Following Using a Small Autonomous Aircraft", *IEEE Aerospace Conference*, 2004.

[5] S. Rathinam, Z. Kim, A. Soghikian and R. Sengupta, "Vision Based Following of Locally Linear Structures using an Unmanned Aerial Vehicle", *44th IEEE Conference on Decision and Control, and the European Control Conference*, Dec 12-15, Seville, Spain, 2005.

[6] S. Rathinam, P. Almeida, Z.W. Kim, S. Jackson, A. Tinka, W. Grossman and R. Sengupta, "Autonomous Searching and Tracking of a River using an UAV", *Proceedings of the 2007 American Control Conference*, Jul 11-13, New York City, USA, 2007.

[7] R.S. Holt and R.W. Beard, "Vision-Based Road-Following Using Proportional Navigation", *Journal of Intelligent and Robotic Systems, 57:193-216*, 2010.

[8] J. Egbert and R.W. Beard, "Low Altitude Road Following Constraints Using Strap-down EO Cameras on Miniature Aerial Vehicles", *Proceedings of the 2007 American Control Conference*, Jul 11-13, New York City, USA, 2007.

[9] D.I. Jones and G.K. Earp "Requirements for aerial inspection of overhead electrical power lines", *Proc. 12th International Conf. on Remotely Piloted Vehicles*, Bristol, 1996.

[10] D.I. Jones, I. Golightly, J. Roberts, K. Usher and G.K. Earp, "Power line inspection - an UAV concept", *IEE Forum on Autonomous Systems*, London, 2006.

[11] C.C. Whitworth, A.W.G. Duller, D. Jones and G.K. Earp, "Aerial video inspection of overhead power lines", *Power Engineering Journal*, Feb, 2001.

[12] P. Campoy, P.J. Garcia, A. Barrientos, J. del Cerro, I. Aguirre, A. Roa, R. Garcia and J.M. Munoz, "An Stereoscopic Vision System Guiding an Autonomous Helicopter for Overhead Power Cable Inspection", Robot Vision, *Robot Vision, Lecture Notes in Computer Science pp. 115-124*, Springer-Verlag.

[13] Z. Li, Y. Liu, R.F. Hayward, J. Zhang, J. Cai, "Knowledge-based Power Line Detection for UAV Surveillance and Inspection Systems", *23rd International Conference on Image and Vision Computing New Zealand (IVCNZ 2008)*, Nov 26-28, Christchurch, New Zealand, USA, 2008.

[14] D. Johanson, J. Hall, C. N. Taylor and R. W. Beard, "Stabilization of video from miniature air vehicles", *Proceedings of the AIAA Conference on Guidance, Navigation and Control*, Hilton Head, South Carolina, USA, 2007.

[15] M. Kontitsis, K. Valavanis and N. Tsourveloudis, "A UAV vision system for airborne surveillance", *Proceedings of IEEE ICRA*, vol. 1, pp. 77-83, 2004.

[16] R.W. Beard, J.W. Curtis, M. Eilders, J. Evers and J.R. Cloutier, "Vision Aided Proportional Navigation for Micro Air Vehicles", *AIAA Guidance, Navigation and Control Conference and Exhibit*, Aug 20-23, Hilton Head, South Carolina, 2007.

[17] N. Yokoyama and Y. Ochi, "Optimal Path Planning for Skid-to-Turn Unmanned Aerial Vehicle", *AIAA Guidance, Navigation and Control Conference and Exhibit*, Aug 18-21, Honolulu, Hawaii, 2008.

[18] E. Frazzoli, M.A. Dahleh, and E. Feron, "Maneuver-Based Motion Planning for Nonlinear Systems With Symmetries", *IEEE Transaction on Robotics*, Vol. 21, No. 6, Dec. 2005.

[19] G. Ambrosino, M. Ariola, U. Ciniglio, F. Corraro, E. De Lellis, and A. Pironti, "Path Generation and Tracking in 3-D for UAVs", *IEEE Transactions on Control Systems Technology*, July, Vol. 17, No. 4, 2009.

[20] P.K. Menon and E.J. Ohlmeyer, "Integrated design of agile missile guidance and autopilot systems", *Control Engineering Practice*, Vol. 9, pp. 1095-1106, 2001.

[21] K.L. Lee, M.A. Langehough and R.A. Chamberlain, "Modern control of bank-to-turn autopilot for Have Dash II Missile", *IEEE Conference on Control Applications*, 1992.

[22] E.P. Anderson, R.W. Beard and T.W. McLain, "Real-Time Dynamic Trajectory Smoothing for Unmanned Air Vehicles", *IEEE Transactions on Control Systems Technology*, Vol. 13, No. 3, May. 2005.

[23] T. Yamasaki, H. Sakaida, K. Enomoto, H. Takano and Y. Baba, "Robust Trajectory-Tracking Method for UAV Guidance Using Proportional Navigation", *International Conference on Control, Automation and Systems*, Oct 17-20, Seoul, Korea, 2007.

[24] M. Niculescu, "Lateral track control law for Aerosonde UAV", *Proceedings of the 39th AIAA Aerospace Sciences Meeting and Exhibit*, 2001.

[25] D.R. Nelson, D.B. Barber, T.W. McLain and R.W. Beard, "Vector Field Path Following for Small Unmanned Air Vehicles", *Proceedings of the 2006 American Control Conference*, Jun 14-16, Minneapolis, Minnesota, USA, 2006.

[26] W. Ren and R.W. Beard, "Trajectory Tracking for Unmanned Air Vehicles With Velocity and Heading Rate Constraints", *IEEE Transactions on Control Systems Technology*, Vol. 12, No. 5, May. 2004.

[27] D. McLean, Automatic Flight Control Systems, Prentice Hall, New York, 1990.

[28] J.R. Cloutier and D.T. Stansbery, "Nonlinear Hybrid Bank-to-Turn/Skid-to-Turn Missile Autopilot Design", *AIAA Paper 2001-4158*, Aug. 2001.

[29] M. Xin, S.N. Balakrishnan, D.T. Stansbery and E.J. Ohlmeyer, "Nonlinear Missile Autopilot Design with θ-D Technique", *Journal of Guidance, Control, and Dynamics*, Vol. 27, No. 3 May-June 2004.

[30] J. Ford, "Precision Guidance with Impact Angle Requirements", *Aeronautical and Maritime Research Laboratory, Defence Science and Technology Organisation, 2001.*

[31] J.Z. Ben-Asher and I. Yaesh, *Advances in Missile Guidance Theory*, American Institute of Aeronautics and Astronautics, Progress in Astronautics and Aeronautics, Vol. 180, Virginia, 1999.
[32] J.Z. Ben-Asher and I. Yaesh, *Advances in Missile Guidance Theory*, American Institute of Aeronautics and Astronautics, Progress in Astronautics and Aeronautics, Vol. 180, Virginia, 1999, Ch. 3.
[33] R.F. Stengel, *Flight Dynamics*, Princeton University Press, Princeton, 2004.
[34] R.F. Stengel, *Flight Dynamics*, Princeton University Press, Princeton, 2004, p. 166.
[35] R.F. Stengel, *Flight Dynamics*, Princeton University Press, Princeton, 2004, p. 55.
[36] N. Ceccarelli, J.J. Enright, E. Frazzoli, S.J. Rasmussen and C.J. Schumacher "Micro UAV Path Planning for Reconnaissance in Wind", *Proceedings of the 2007 American Control Conference*, July 11-13, New York, USA.
[37] H.J. Kushner and P. Dupuis, *Numerical Methods for Stochastic Control Problems in Continuous Time*, 2nd Ed. Springer-Verlag, New York, 2001.
[38] J. J. Ford, "Optimal stopping time guidance: deterministic and stochastic targets," in Control Conference, 2004. 5th Asian, Vol. 3, pp. 1826-1832, 2004.
[39] M. Sadraey, R. Colgren, "UAV Flight Simulation: Credibility of Linear Decoupled vs. Nonlinear Coupled Equations of Motion", *AIAA Conference*, Aug, San Francisco, 2005.
[40] Laminar Research. (2010, Jun). [Online]. X-plane. Available: http://www.x-plane.com

Troy S. Bruggemann was born in Nambour, Australia in 1981. He completed a B. E. (aerospace avionics) in 2002, M. Eng. in 2005 and PhD in 2009 from the Queensland University of Technology (QUT). Since 2009 he has held a postdoctoral research fellow position within the Australian Research Centre for Aerospace Automation (ARCAA) at QUT. His research interests include navigation and control for aerospace.

Jason J. Ford was born in Canberra, Australia in 1971. He received the B.Sc. and B.E. degrees in 1995 and a PhD in 1998 from the Australian National University, Canberra. He was appointed a research scientist at the Australian Defence Science and Technology Organisation in 1998, and then promoted to a senior research scientist in 2000. He has held research fellow positions at the University of New South Wales at the Australian Defence Force Academy in 2004, and at the Queensland University of Technology in 2005. He was appointed a lecturer at the Queensland University of Technology in 2007, and then promoted to senior lecturer in 2010. His research interests include signal processing and control for aerospace.

Rodney A. Walker became a Member of the IEEE in 2001 and was born in Cairns, Australia in 1969. He completed Bachelor degrees in Engineering (electronic systems) and Applied Science (computing) from the Queensland University of Technology in 1992. He completed his PhD in satellite navigation from the same institution in 1999 after spending a year studying at the Rutherford Appleton Laboratory in the UK. From 1998 to 2005 he was responsible for the GPS payload on Australia's Federation Satellite working closely with NASA JPL during this time. Since 2000 he has directed his interests to ICT in aviation and created the Australian Research Centre for Aerospace Automation (ARCAA) which now has over 30 full-time staff. He is also a private pilot with NVFR and Aerobatics endorsements.